Research Article

Guido Maione*

Fractional-order lead networks to avoid limit cycle in control loops with dead zone and plant servo system

https://doi.org/10.1515/nleng-2022-0357
received September 21, 2023; accepted November 20, 2023

Abstract: The fractional-order controllers (FOCs) have recently had a significant impact on control applications. However, they still need further research for feedback systems with hard nonlinearities, such as dead zones. The above compelling evidence motivates the design of a new robust FOC to avoid limit cycles caused by dead zones in the control loops. The proposed FOC consists of the cascade of two shifted in frequency, fractional-order lead networks. They provide high-value and sufficiently flat phase leads in sufficiently large frequency intervals. In this way, the linear part of the control loop can be easily shaped to achieve avoidance of limit cycles. The article applies classical concepts, such as the Nyquist plot and describing function method, to derive guidelines for designing the free parameters of the FOC. Moreover, a realization algorithm and a parameter setting procedure make the new FOC easily implementable in engineering practice.

Keywords: fractional-order lead networks, nonlinear control systems, dead zone, limit cycle, describing function

MSC 2020: 93B52, 93Cxx, 93C10, 70K05, 93B51, 93C80

1 Introduction

Control systems are negatively affected by the dead zone nonsmooth nonlinearity, which produces poor steady-state accuracy, limit cycles, and system instability [1]. Besides, the dead zone nonlinearity (DZNL) is difficult to remove because it is described by nondifferentiable models with poorly known parameters [2]. For this reason, the pioneered adaptive inverse schemes used by [1,3,4] in combination with many control design approaches do not achieve the perfect cancellation of the DZNL but only obtain bounded output errors [5]. Other attempts to compensate for the DZNL have also been made by neural networks [6] and fuzzy logic methods [7]. However, on the one hand, the above techniques are usually not suited for industrial practice because of the heavy computational demand, but, on the other hand, the common proportional-integral-derivative (PID) controllers cannot face the challenges of nonlinear control problems.

Recently, the so-called fractional-order controllers (FOCs for brevity), which are based on noninteger orders of integration and differentiation, have been proposed and, in many cases, gradually replaced the standard PID controllers in solving complex problems. Since they use integrators and differentiators of noninteger orders, the FOCs introduce two more tuning parameters for improving the performance of the classical PID controllers. Moreover, it is remarked that fractional derivatives and fractional-order differential equations offer an enhanced and more flexible tool to mathematical modeling than integer-order differential equations [8,9]. These fundamental reasons motivated the success of pioneering applications. The Commande Robuste d'Ordre Non Entièr [10,11] has made relevant contributions to the automotive industry, and the $PI^{\lambda}D^{\mu}$-controller [12] has generalized and made more flexible the PID controller. Moreover, in the tilted integral derivative controller [13], the operator $s^{1/n}$ (with n integer) has successfully controlled systems with uncertain parameters. Finally, the fractional lead-lag networks have shown better robustness and flexibility than their integer counterparts [14,15]. Auto-tuning was also developed [15,16], and neural networks were employed for the design and implementation of noninteger-order integrators [17].

However, the FOCs still need further research in nonlinear applications. In this context, starting from the combination of fractional calculus and sliding-mode control for integer-order systems [18] or fractional-order systems [19], some contributions exist for sliding-mode control of certain classes of uncertain linear [20] or nonlinear fractional-order systems [21]. It is also recalled that nonlinear chaotic

* **Corresponding author: Guido Maione,** Department of Electrical and Information Engineering, Polytechnic University of Bari, Via E. Orabona, 4, I-70125, Bari, Italy, e-mail: guido.maione@poliba.it

systems can be of noninteger (fractional) order, and the topic of chaos synchronization is investigated very much because of the benefits in different areas of science and engineering [22,23]. However, in some cases, chaos is not desirable, and control is designed to suppress the chaotic oscillations of the fractional-order uncertain model of real systems like a permanent magnet synchronous generator [24].

In particular, with a nonlinear element in the control loop, the FOCs require specific control algorithms for industrial practice [25]. Hence this article introduces a new, two-stage controller – represented by the transfer function $H_{12}(s)$ – to avoid the occurrence of limit cycles due to a DZNL. The controller is made by two fractional-order lead networks, which are shifted in frequency relatrive to each other. The uncompensated system including the nonlinear dead zone element and a linear plant represented by a transfer function $G_p(s)$, namely a servo system, can show a limit cycle. (By the way, nonlinear systems are frequently represented by the series of a memoryless nonlinearity and a linear transfer function, and the derived Hammerstein model is important in control engineering, since it can effectively approximate many devices [26,27].) Otherwise, the scheme in Figure 1 describes the system compensated by the FOC. The controller $H_{12}(s)$ consists of a cascade of two shifted fractional-order lead networks (an SFLN for brevity) that are placed at a given distance, one after the other, on the frequency axis. By providing a nearly constant phase in a sufficiently large frequency interval, the SFLNs inhibit the intersections between the plots of the negative inverse of the dead zone describing function and the loop transfer function, given that such intersections are necessary conditions for a limit cycle to occur. Finally, the design and rational realization of the SFLNs is easy and guarantees a secure and robust avoidance of limit cycles in servo systems with a dead zone in the control loop.

The organization of this article is as follows: Section 2 describes the proposed FOC, which is an irrational, two-stage fractional-order lead network made of two consecutive stages, and moreover, the section shows the realization of the controller by a rational transfer function; Section 3 introduces a design approach of the proposed SFLN and gives an illustrative example at the same time; and Section 4 gives the conclusions.

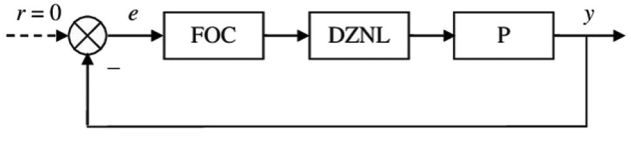

Figure 1: The compensated control system: FOC is the fractional-order controller compensating the DZNL and P is the plant having transfer function $G_p(s)$.

2 The controller: two shifted in frequency fractional-order lead networks

2.1 Formalization and properties of the controller

Analytic formulas have made the design of a classical, integer-order lead network easy, mainly because the mathematical expressions relate the controller parameters to the frequency of the maximum phase lead. In the frequency domain, this relation is important because the maximum lead has to fall exactly at the gain crossover frequency of the compensated system. Unfortunately, it is not easy to find similar relationships for general multiple-stage, shifted in frequency, fractional-order lead networks. However, if the analysis is restricted to two-stage SFLNs, the next arguments show that the frequency (u_{m12}) of the maximum lead is the real, positive root of a linear, irreducible, cubic equation. Moreover, the coefficient values of the Cardano's equation depend on the SFLN parameters. To prove the above statement, consider the transfer functions of the first and second stages that are, respectively, $H_1(s) = \left(\frac{1+\tau s}{1+\tau\Delta s}\right)^{\nu_1}$ and $H_2(s) = \left(\frac{1+\tau F s}{1+\tau F\Delta s}\right)^{\nu_2}$, where $\nu_1 = \nu_2 = \nu$ is set to obtain equal but shifted stages. Here, τ and $\tau\Delta$ are the numerator and denominator time constants (in seconds) of the first stage, F represents the shift of the second stage with respect to the first, and the noninteger (fractional) exponent ν, with $0 < \nu < 1$, is the so-called fractional order. Then, the frequency response of the two-stage SFLN is given as follows:

$$H_{12}(ju) = H_1(ju)H_2(juF) = \left(\frac{1+ju}{1+ju\Delta}\right)^{\nu}\left(\frac{1+juF}{1+juF\Delta}\right)^{\nu}, \quad (1)$$

where the variable $u = \omega\tau$ is the dimensionless angular frequency and ω is the angular frequency (in radians/seconds). The minimum value of Δ in a classical lead network can be fixed to 0.05 because it is limited by the physical construction of the compensator and by the limitations of the maximum phase lead and high-frequency gain that are provided by the network [28]. Namely, if a maximum phase lead greater than 60° is needed, two cascaded lead networks with moderate values of Δ are advised. Moreover, high-frequency noise signals are amplified by $1/\Delta$, while a unitary amplification applies to low-frequency control signals. Then, $\Delta > 0.07$ is often recommended [29]. The usual choice is $\Delta \in (0.05, 0.25)$ [28,29]. Then, this

article makes the common choice $\Delta = 0.1$, which is recommended for lead networks [29], for both stages of the proposed SFLN.

Finally, the parameter F, with $0 < F < 1$, shifts the phase diagram of $H_2(juF)$ with reference to the position of the phase diagram of $H_1(ju)$ on the u-axis [30–32]. Clearly, the fractional-order lead networks, $H_1(ju)$ and $H_2(juF)$, provide their maximum phase leads at the frequencies $u_{m1} = 1/\sqrt{\Delta}$ and $u_{m2} = 1/(F\sqrt{\Delta})$, respectively. These values coincide with the frequencies at which the maximum phase lead occurs in a network with the same base but with an integer-order exponent $\nu = 1$. They are also the geometric mean of the two corner frequencies, *i.e.*, the middle point, in the logarithmic scale, between the zero and pole corner frequency. So, according to De Moivre's theorem, the phase of $H_1(ju)$ at $u = u_{m1}$ has the value $\Phi_{m1} = \angle H_1(ju_{m1})$ given as follows:

$$\begin{aligned}\Phi_{m1} &= \nu[\tan^{-1}(u_{m1}) - \tan^{-1}(u_{m1}\Delta)] \\ &= \nu \tan^{-1}\left(\frac{u_{m1}(1-\Delta)}{1+u_{m1}^2\Delta}\right) \\ &= \nu \tan^{-1}\left(\frac{1-\Delta}{2\sqrt{\Delta}}\right).\end{aligned} \tag{2}$$

Similarly, the second stage provides the maximum value $\Phi_{m2} = \angle H_2(ju_{m2}F)$ at the frequency $u = u_{m2} = 1/(F\sqrt{\Delta})$, with

$$\begin{aligned}\Phi_{m2} &= \nu \tan^{-1}\left(\frac{u_{m2}F(1-\Delta)}{1+u_{m2}^2F^2\Delta}\right) \\ &= \nu \tan^{-1}\left(\frac{1-\Delta}{2\sqrt{\Delta}}\right) \\ &= \Phi_{m1}.\end{aligned} \tag{3}$$

Moreover, if two generic frequencies u_1 and u_2, with $u_1 < u_2$, satisfy the relationship $u_1 = u_2F$, then similar arguments easily show that $\angle H_1(ju_1) = \angle H_1(ju_2F) = \angle H_2(ju_2)$.

Now the frequency u_{m12}, where $H_{12}(ju)$ provides the maximum phase lead, say Φ_{m12}, must be determined. Namely, the pair (u_{m12}, Φ_{m12}) plays a major role in an SFLN design finalized to both avoiding the limit cycle and maintaining the stabilization mode. To determine u_{m12}, the following equation must be solved:

$$\frac{\mathrm{d}}{\mathrm{d}u}\angle H_{12}(ju) = \frac{\mathrm{d}}{\mathrm{d}u}[\angle H_1(ju) + \angle H_2(juF)] = 0. \tag{4}$$

Since $\angle H_1(ju) = \nu[\tan^{-1}(u) - \tan^{-1}(u\Delta)]$ and $\angle H_2(juF) = \nu[\tan^{-1}(uF) - \tan^{-1}(uF\Delta)]$, we obtain:

$$\frac{1-u^2\Delta}{(1+u^2)(1+u^2\Delta^2)} + \frac{F(1-u^2F^2\Delta)}{(1+u^2F^2)(1+u^2F^2\Delta^2)} = 0. \tag{5}$$

After simple but tedious calculations, Eq. (5) and the positions $\alpha = F\Delta$, $\beta = (1+\Delta^2)$, and $\gamma = (1 - F + F^2)$ lead to:

$$\alpha^3u^6 + \alpha(\beta F - \gamma\Delta)u^4 - (\beta F - \gamma\Delta)u^2 - 1 = 0. \tag{6}$$

So putting $u^2 = q$ in Eq. (6), an obvious choice of symbols leads to

$$q^3 + c_1q^2 + c_2q + c_3 = 0, \tag{7}$$

with

$$\begin{aligned}c_1 &= \frac{\beta F - \gamma\Delta}{(F\Delta)^2}, \\ c_2 &= -\frac{\beta F - \gamma\Delta}{(F\Delta)^3}, \\ c_3 &= -\frac{1}{(F\Delta)^3}.\end{aligned} \tag{8}$$

The coefficients of Eq. (8) only depend on F and Δ and can be easily determined. Since c_1, c_2, and c_3 are real, Eq. (7) has at least one real root. Moreover, by Descartes' *Rule of signs*, the number of positive real roots of Eq. (7) is either equal to the sign changes in the sequence $\{1, c_1, c_2, c_3\}$ or is less than this number by a positive even integer [33]. The values $F \in (0.1, 1)$ and $\Delta = 0.1$ used by this article (see next section), give $c_1 > 0$, $c_2 < 0$, and $c_3 < 0$, so that the number of sign variations is 1. Hence, Eq. (7) has exactly one real positive root (say q_1). The value of q_1 can be obtained as a numerical solution of Eq. (7) or as a result of Cardano's analytical procedure [34] and leads to the frequency of the maximum phase lead. In this article, q_1 is obtained as a numerical solution of Eq. (7). Hence, $u_{m12} = \sqrt{q_1}$.

Now comments on further characteristics of $H_{12}(ju)$ are in order. The following analysis tries to fix the fractional order ν on the basis of preliminary design decisions. Thus, to provide the phase lead the control loop requires for compensation, the value of ν is first selected. For example, in the case of the next section, a good first choice is $\nu = 0.7$. Moreover, the parameters F and Δ influence u_{m12} and $\Phi_{m12} = \angle H_{12}(ju_{m12})$, which are the main frequency-domain measures assessing performance. Hence, if Δ is fixed (e.g., $\Delta = 0.1$), each value given to F will identify a member $\Phi_{12}(u, F) = \angle H_{12}(ju) = f_F(u)$ of a function family. As shown in Figure 2, each phase-frequency plot is marked by an F-value. Moreover, the lower values of F make the phase curves flatter around their maximum, Φ_{m12}, whereas the more the value of F rises, the more Φ_{m12} increases and u_{m12} decreases (Figure 2 and Table 1).

In the second relation, each value assigned to Δ leads to a one-to-one function $u_{m12}(F, \Delta) = f_\Delta(F)$ and to a curve of Figure 3. Lower values of Δ lead to higher values of u_{m12} corresponding to assigned F.

Figures 2 and 3 with formulas (6), (7), and (8) are the basis of an efficient grapho-analytical design procedure of $H_{12}(ju)$. Of course, different pairs of the above figures can be obtained for different values of the fractional order ν.

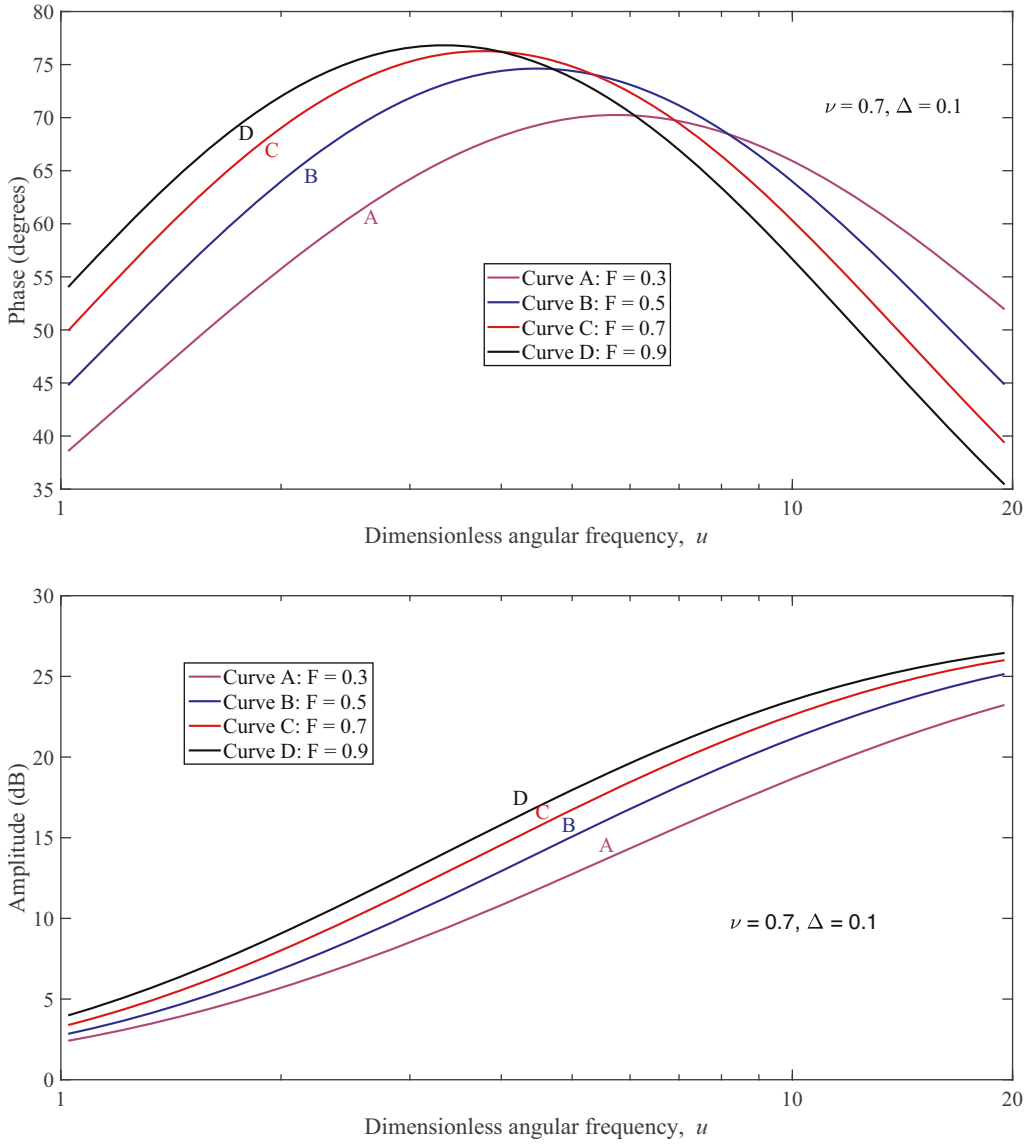

Figure 2: Phase and amplitude Bode diagrams of $H_{12}(ju)$ as a function of u and for different values of F, with $\nu = 0.7$ and $\Delta = 0.1$.

2.2 Realization of the controller

The model of the SFLN is irrational and infinite-dimensional. However, a finite-dimensional, rational transfer function realization can be obtained in three steps. The first one introduces the rational transfer function approximating the irrational derivative operator x^{ν}:

$$x^{\nu} \approx \frac{\sum_{i=0}^{N} b_{N-i} x^{i}}{\sum_{i=0}^{N} a_{N-i} x^{i}}, \tag{9}$$

where $x \in \mathbb{C}$ (complex plane) and $0 < \nu < 1$. Note that the coefficients a_{N-i} and b_{N-i} depend on ν and can be obtained by one of the existing methods (see [35] and references therein). However, this article proposes the following simple, effective closed-formulas for a_{N-i} and b_{N-i}:

$$b_i = a_{N-i} = (-1)^i \binom{N}{i} (\nu + i + 1)_{(N-i)} (\nu - N)_{(i)} \qquad i = 0, 1, 2, \ldots, N, \tag{10}$$

Table 1: Maximum phase lead and its dimensionless angular frequency

F	u_{m12}	Φ_{m12}
0.3	5.77	70.2°
0.5	4.47	74.6°
0.7	3.78	76.3°
0.9	3.33	76.8°

where

$$(\nu + i + 1)_{(N-i)} = (\nu + i + 1)(\nu + i + 2)\cdots(\nu + N) \quad (11)$$

$$(\nu - N)_{(i)} = (\nu - N)(\nu - N + 1)\cdots(\nu - N + i - 1) \quad (12)$$

define the Pochhammer functions, with $(\nu + N + 1)_{(0)} = (\nu - N)_{(0)} = 1$ (see [36,37] for more details). In the second step, the transformation

$$x = \frac{1 + \tau s}{1 + \Delta\tau s} \quad (13)$$

is introduced in Eq. (9). Then, some elementary operations lead to:

$$\begin{aligned} H_1(s) &= \left(\frac{1 + \tau s}{1 + \Delta\tau s}\right)^{\nu} \approx G_1(s) \\ &= \frac{\sum_{i=0}^{N} b_{N-i}(1 + \tau s)^i(1 + \Delta\tau s)^{N-i}}{\sum_{i=0}^{N} a_{N-i}(1 + \tau s)^i(1 + \Delta\tau s)^{N-i}}. \end{aligned} \quad (14)$$

Furthermore, a routine-based algebra yields

$$G_1(s) = \frac{\sum_{k=0}^{N} B_{N-k}s^k}{\sum_{k=0}^{N} A_{N-k}s^k}, \quad (15)$$

where A_{N-k} (B_{N-k}) depends on a_{N-i} (b_{N-i}) according to the following linear combination:

$$A_{N-k} = \tau^k \sum_{i=0}^{N} a_{N-i}L_{ki} \quad (16)$$

with

$$\begin{aligned} L_{ki} &= \sum_{m=m_1}^{m_2} \binom{i}{m}\binom{N-i}{k-m}\Delta^{k-m} \\ &= \sum_{m=m_1}^{m_2} \binom{i}{i-m}\binom{N-i}{N-i-k+m}\Delta^{k-m}, \end{aligned} \quad (17)$$

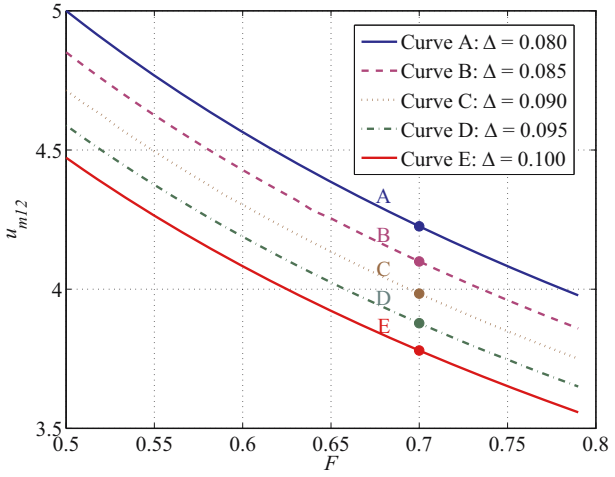

Figure 3: Value of the dimensionless angular frequency $u_{m12}(F, \Delta)$ for the maximum phase lead as function of F and with $\nu = 0.7$.

and where $m_1 = \max\{0, k + i - N\}$ and $m_2 = \min\{i, k\}$ because of the restriction imposed by the binomial coefficients: $0 \le m \le i$ and $0 \le k - m \le N - i$ [30].

In the third step, the rational transfer function of the second stage $H_2(s)$ can be immediately obtained by replacing s with Fs:

$$H_2(s) \approx G_2(s) = \frac{\sum_{k=0}^{N} B_{N-k}(Fs)^k}{\sum_{k=0}^{N} A_{N-k}(Fs)^k}. \quad (18)$$

In conclusion, $H_{12}(s) \approx G_1(s)G_2(s)$.

Figures 2 and 4 show the amplitude and phase plots of an SFLN with some values assigned to ν and Δ. Figure 4 shows a fourth-order ($N = 4$) approximation by a dash-dotted line. Note that the discrepancy between the irrational network $H_{12}(j\omega)$ and its approximation $G_1(j\omega)G_2(j\omega)$ in the Bode phase diagram is not important. Namely, it is negligible for $u < u_{m12}$ and gives no problem for $u = u_{m12}$, where the maximum phase Φ_{m12} is achieved and used for design purpose (Section 3). The phase difference only consists in few degrees for $u > u_{m12}$, but it does not significantly affect the design that requires specifications at u_{m12} and a certain flatness in the immediate range around u_{m12}.

As for the phase plot concerns, curve C ($F = 0.7$) in Figures 2 and 4 shows a sufficiently flat phase behavior in a sufficiently large frequency range both for the irrational controller $H_{12}(s)$ and for its rational transfer function realization. The phase diagram is not really "flat" (constant phase) but its variation is limited, especially with reference to the corresponding phase change provided by integer-order networks.

3 Robust controller design to avoid the limit cycle

3.1 The system with limit cycle

This section proposes the positional control of a common type of plant, *i.e.*, a servomotor, as case study (Figure 5). The transfer functions of the controller $H_{12}(s)$ and servomotor $G_p(s)$ are the constituent linear parts of the control loop. Preliminarily, however, Figure 5(a) is considered without $H_{12}(s)$ to point out the presence of limit cycles in the autonomous system (with $r = 0$) including a memoryless time-invariant nonlinearity. So let

$$G_p(s) = \frac{K_p}{s(1 + T_1 s)(1 + T_2 s)} \quad (19)$$

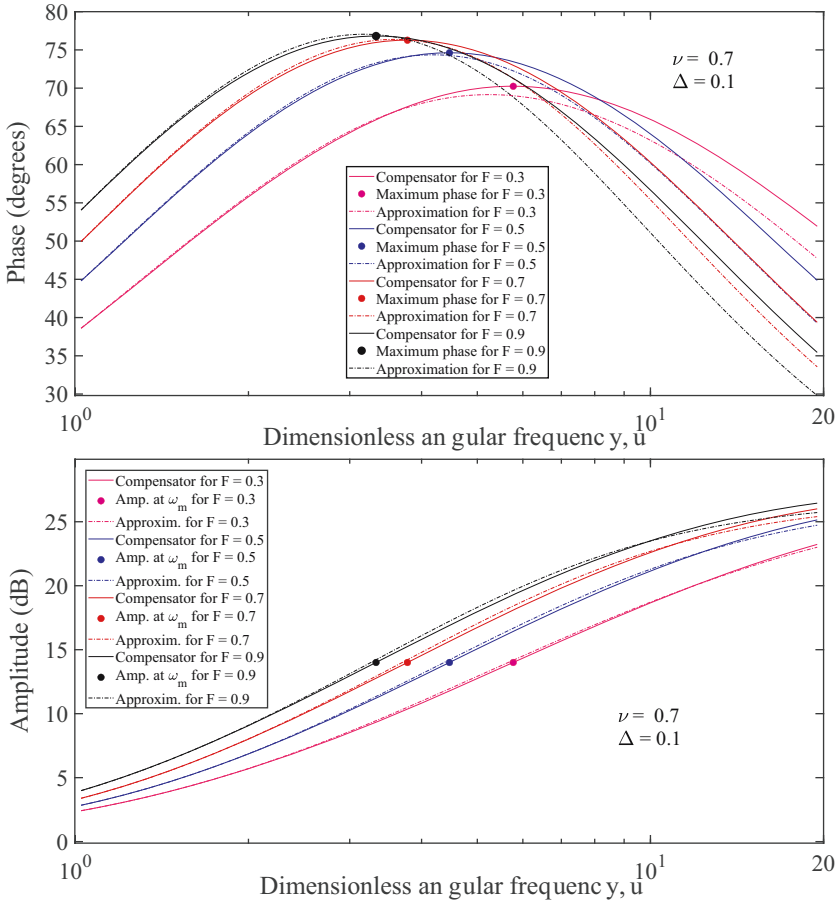

Figure 4: Phase and amplitude Bode diagrams of $H_{12}(ju)$ (continuous line) and $G_1(ju)G_2(ju)$ (dashed line).

with K_p = 10, T_1 = 0.15 s, and T_2 = 0.95 s. Without $H_{12}(s)$, at the phase and gain crossover frequencies (ω_{pcP} = 2.65 rad/s and ω_{gcP} = 3.01 rad/s), respectively, the values of the gain and phase margins of $G_p(j\omega)$ are poor (*i.e.*, GM_P = 0.77 and PM_P = −5.02°).

Moreover, a DZNL in the loop is described as follows:

$$z = \begin{cases} \mu(w + a) & \text{for } w < -a \\ 0 & \text{for } -a \le w \le a \\ \mu(w - a) & \text{for } w > a, \end{cases} \tag{20}$$

where μ = 1 and a = 0.8 are here used, w is the input to the dead zone, z is the output from the dead zone, and Figure 5(a) explains the meaning of the symbols μ (slope) and a (half of dead zone).

Now the describing function approach can be successfully applied because, by replacing $s \to j\omega$ in Eq. (19), $G_p(j\omega)$ shows the necessary higher harmonics filtering capacity. Hence, the harmonic balance equation yields

$$G_p(j\omega) = -\frac{1}{N(W)} = V(W), \tag{21}$$

where W is the amplitude of the sinusoidal input $w(t) = W\sin(\omega t)$ applied to the nonlinear element and

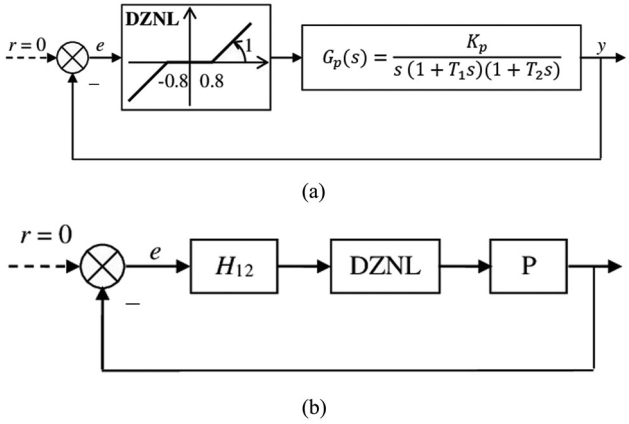

Figure 5: Block schemes describing the FOC of a servomotor with a dead zone. (a) The uncompensated system including the DZNL with μ = 1 and a = 0.8 and the plant transfer function $G_p(s)$ and (b) the controlled system: $H_{12}(s)$ is the controller with two, shifted in frequency, fractional-order lead networks, DZNL is the dead zone nonlinearity, and P is the plant.

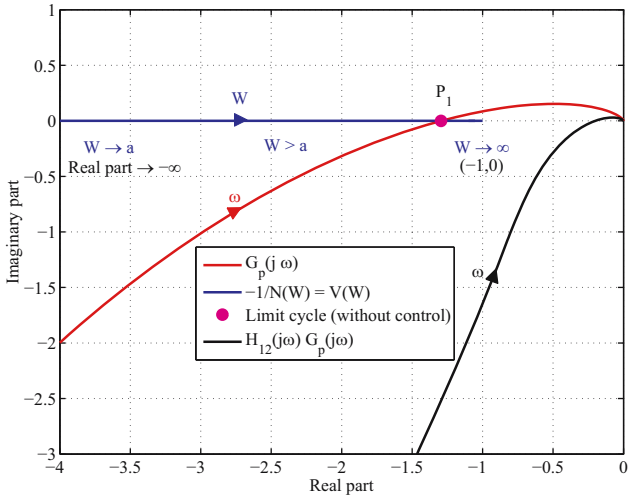

Figure 6: Nyquist plot of $G_p(j\omega)$ (red solid line); negative inverse of the describing function of the DZNL (blue solid line); point $P_1(W_c, \omega_c)$: limit cycle position; Nyquist plot of $H_{12}(j\omega)G_p(j\omega)$ (black solid line): no limit cycle occurs.

$$N(W) = \begin{cases} 0 & \text{for } W \le a \\ \mu\left[1 - \frac{2}{\pi}\sin^{-1}\left(\frac{a}{W}\right) - \frac{2a}{\pi W}\sqrt{1 - \left(\frac{a}{W}\right)^2}\right] & \text{for } W > a \end{cases} \quad (22)$$

is the describing function of the DZNL element [38,39]. Since the dead zone is a single-valued nonlinearity, $N(W)$ and its negative inverse $V(W)$ are real and their plots lie on the real axis (Figure 6). Moreover, the intersection point P_1 of the curve $G_p(j\omega)$ and the curve $V(W)$ corresponds to a limit cycle that is defined by the pair (W_c, ω_c), with $N(W_c) = (T_1 + T_2)/(K_p T_1 T_2)$ and $\omega_c = 1/\sqrt{T_1 T_2}$. The amplitude W_c corresponds to P_1 on the $V(W)$ curve, and the same point P_1 on the plot of $G_p(j\omega)$ identifies the limit cycle frequency, ω_c (Figure 6). In this case, it holds $(W_c, \omega_c) = (4.42, 2.65)$. The curve $V(W)$ plays the role of a "critical curve" that is comparable to the critical point $(-1 + j0)$ in the simplified Nyquist stability criterion [38], according to Eq. (21) and the simplified scheme in Figure 5(a). Then, if no control is applied, the time-domain control system response exhibits a limit cycle oscillation, as shown in Figure 7. Finally, since the plot of $V(W)$ meets the curve of $G_p(j\omega)$ from left to right of the cross-point P_1, then a practical rule states that the limit cycle is unstable [38,40]. As remarked in [39], the importance of the Nyquist plot and Nyquist criterion in control theory made the graphical implementation of the describing function method a popular tool available to control engineers, when facing nonlinear control systems [39].

3.2 Controller design

The robust limit cycle avoidance is committed both to the Gain Margin (GM) and Phase Margin (PM) of $G_{HP}(j\omega) = H_{12}(j\omega)G_p(j\omega)$. Namely, one or another between the PM and GM is a suitable design metric because $G_{HP}(j\omega)$ is minimum-phase with a unique relation between the amplitude and phase. Hence, the controller $H_{12}(j\omega)$ must shape $G_{HP}(j\omega)$ to make the compensated Nyquist plot be at a suitable distance from $P_1(W_c, \omega_c)$.

However, some difficulties arise. Namely, combining $H_{12}(j\omega)$ in cascade with $G_p(j\omega)$ shifts the gain crossover frequency of $G_{HP}(j\omega)$, say ω_{gcHP}, on the right of the gain crossover frequency ω_{gcP} of $G_p(j\omega)$. Hence, $H_{12}(j\omega)$ must provide additional leads to compensate for the larger

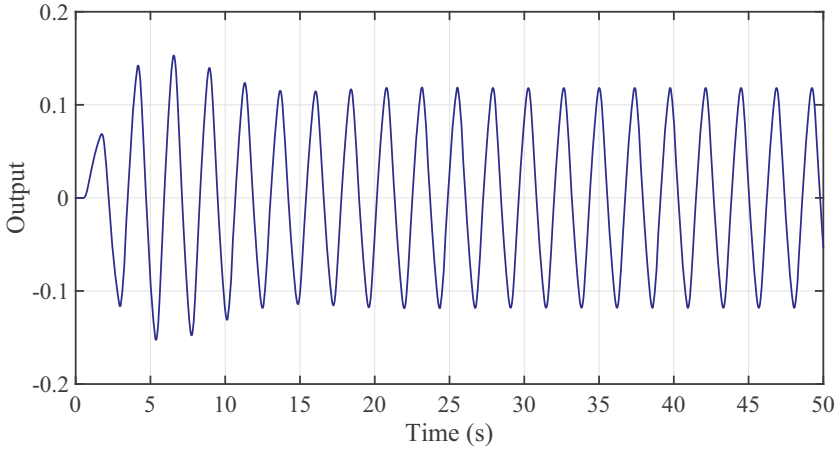

Figure 7: Output oscillation (limit cycle) when no control is applied.

phase lag introduced by $G_p(j\omega)$ at $\omega = \omega_{gcHP}$. A well-established practice suggests an increment of $\varepsilon = 20°\sim25°$ to the specified desired margin (*i.e.*, to $PM_s = 40°\sim50°$) [29]. The choice of the controller parameters of $H_{12}(j\omega)$ is in six steps.

1) *First step: setting Δ.* To begin with, the value of Δ is chosen for $H_{12}(j\omega)$. In common, integer-order, phase lead networks, the value $\Delta = 0.1$ reaches a good compromise between the phase request and an acceptable sensitivity to high-frequency noise [40]. Hence, the same value is chosen for $H_{12}(j\omega)$, as it was shown and anticipated in Section 2.
2) *Second step: setting ν and F to obtain a specified phase margin.* The values of the parameters F and ν must guarantee both a phase margin of the system $G_{HP}(j\omega) = H_{12}(j\omega)G_p(j\omega)$, namely $PM_{HP} = PM_s \geq 40°\sim50°$, and a nearly flat-phase interval. Hence, to compensate a large phase lag at the (still unknown) gain crossover frequency ω_{gcHP} of the open-loop transfer function $G_{HP}(j\omega)$, the controller $H_{12}(j\omega)$ should provide a maximum phase lead $\Phi_{m12} = PM_{HP} - PM_P + \varepsilon = 70°\sim75°$. As for ν, since the fractional order deeply affects the phase leads provided by $H_{12}(j\omega)$ (Section 2.2), the required values can suitably be obtained with $\nu \in (0.7, 0.8)$. According to Figure 2, which is drawn for $\nu = 0.7$, the curves A-D, corresponding to some values of F in the range $F \in (0.3, 0.9)$, guarantee the required leads with nearly flat phase patterns around the frequency of the maximum phase lead. Since flatter curves correspond to lower leads, flatness and phase lead values must be balanced. Hence, after some attempts, $F = 0.7$ and $\nu = 0.7$ are chosen so as to obtain both the maximum lead $\Phi_{m12} = 76.3°$ in correspondence of $u_{m12} = 3.78$ and a flat phase in a given frequency interval (Figure 3 and Table 1).
3) *Third step: computing the shift of the gain crossover frequency*. The time constant τ of the first stage $H_1(j\omega) = \frac{1+j\omega\tau}{1+j\omega\tau\Delta}$ of $H_{12}(j\omega)$ is chosen so that the maximum lead of the controller will contribute wholly to the phase margin. Hence, let $\tau\omega_{gcHP} = u_{m12}$ and use the parameter $h > 1$ to express ω_{gcHP} in terms of ω_{gcP} as follows: $\omega_{gcHP} = h\omega_{gcP}$. Then, τ can be written as:

$$\tau(h) = \frac{u_{m12}}{h\omega_{gcP}}. \tag{23}$$

   To obtain out of the circular difficulty of determining the (unknown) time constant τ in terms of the (unknown) parameter h, a simple numerical code is used to find the element $h = \bar{h}$ giving both the smallest value $E(\bar{h}) = \min_h|1 - G_{HP}(jh\omega_{gcP})| \cong 0$ and its position in the vector $E(h)$. The result gives $E(\bar{h}) = 0.003$ for $\bar{h} = 2.21$ and $\omega_{gcHP} = \bar{h}\omega_{gcP} = 6.67$ rad/s.
4) *Fourth step: setting time constants of the two stages.* The outcome $\bar{h}$ of the third step gives $\tau = u_{m12}/\omega_{gcHP} = 0.57$ s and $\tau_1 = F\tau = 0.40$ s.
5) *Fifth step: checking the phase margin.* The resulting irrational network $H_{12}(j\omega)$ leads to $\angle G_{HP}(j\omega_{gcHP}) = -132°$ and to the phase margin $PM_{HP} = 48°$. By using the fourth-order, rational transfer function realization $G_1(j\omega)G_2(j\omega)$, the phase margin $PM_{GP} = 45.1°$ is obtained. A better approximation to PM_{HP} can be easily obtained with rational transfer functions of higher order N (Section 2.2).
6) *Sixth step: determination of the phase crossover frequency and gain margin*. To determine the gain margin, the vector $|\angle H_{12}(j\omega)G_p(j\omega) + \pi|$ is defined and its component with minimum value is determined. Based on the previously determined parameters for $H_{12}(j\omega)$, the minimum returns $\angle H_{12}(j\omega_{pcHP})G_p(j\omega_{pcHP}) = -3.15$ radians at the phase crossover frequency ω_{pcHP}. The correspondent $|H_{12}(j\omega_{pcHP})G_p(j\omega_{pcHP})| = 0.20$ leads to the margin $GM_{HP} = 14$ dB.

The gain margin obtained with the controller transfer function $H_{12}(j\omega)$ establishes a useful robustness measure, which shows the efficiency of the design approach. It guarantees a suitable distance between the intersection of the Nyquist plot of the compensated linear part with the negative real axis (square point in Figure 8) and the plot of the negative inverse of the dead zone describing function. Namely, Figure 8 indicates the design robustness to plant parametric variations. Part (a) considers a ±20% change in the plant gain, and part (b) considers a ±20% change in the lower time constant T_1. These changes determine an uncertainty region whose limits are specified by the dashed red curves around the Nyquist plot of $G_p(j\omega)$. Then, the resulting region of the compensated system has limits given by the dashed black curves around the Nyquist plot of $H_{12}(j\omega)G_p(j\omega)$. The first square point on the nominal Nyquist plot (solid line) located between the limit curves intersects the unit circle, thus providing the gain crossover frequency and the phase margin. The second square point on the nominal plot corresponds to the phase crossover frequency and the gain margin. Then, as the figures show, the design is quite robust with respect to parametric variations.

Remark. The controller structure could be extended by introducing a pure integrator, for example, when it is required to reject disturbances on the plant input or to improve steady-state accuracy in reference tracking. Then, the proposed design methodology remains applicable if one treats this integrator as part of the plant transfer function during the control design procedure.

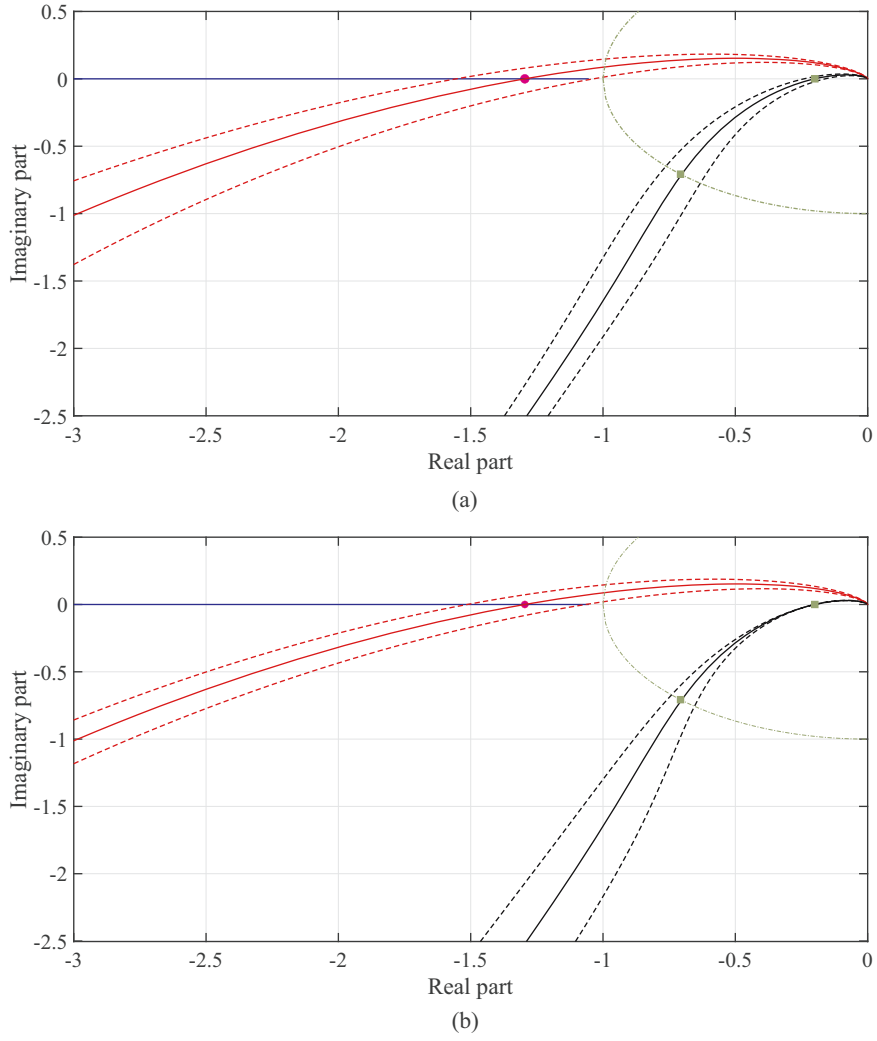

Figure 8: Evaluation of robustness to plant parametric uncertainties. (a) Sensitivity to ±20% variation in the plant gain and (b) sensitivity to ±20% variation in the plant lower time constant.

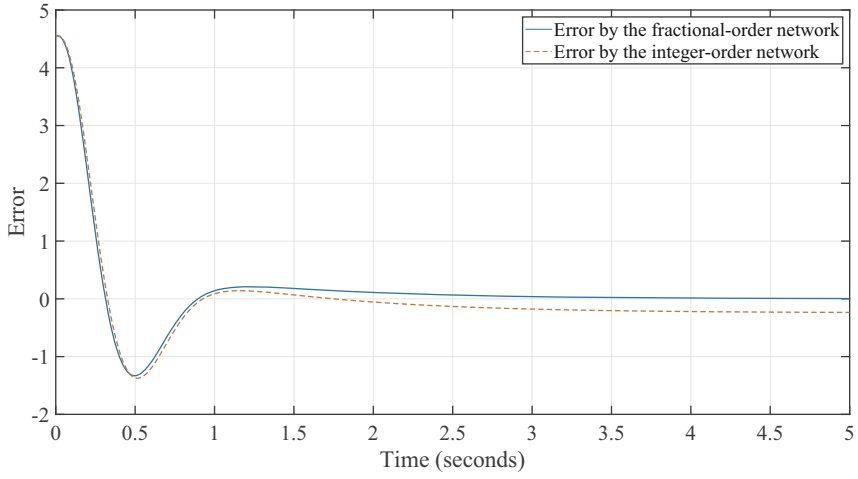

Figure 9: Control error with noninteger-order and integer-order networks.

3.2.1 Integer-order network

An integer-order lead network can be designed by a classical procedure [28,29]. The proposed fractional-order control design draws inspiration from this classical method. In the integer-order case, since the required phase lead (75°) in the example is higher than the maximum achievable by a lead compensator (about 65°), a double integer-order lead network, *i.e.*, two equal lead networks with the same parameters are designed. Then, the controller is represented by $H(s) = \left(\frac{1+\tau_a s}{1+\tau_a \alpha s}\right)^2$. The classical design procedure gives $\alpha = 0.24$ and $\tau_a = 0.36$ s. Then, a phase margin $PM = 45°$ is obtained at $\omega_{gc} = 5.69\,\text{rad/s}$, and the gain margin is $GM = 11.2$ dB at $\omega_{pc} = 13.1$ rad/s. Although the frequency-domain specifications are met and the Nyquist plot does not intersect the plot of the negative inverse of the describing function, the time-domain control error is not satisfactory because the steady-state error is not zero, as shown in Figure 9, where a reference step input $r = 4.5$ is considered to generalize the case of $r = 0$. We may conclude that the integer-order controller is not suitable, thus showing the superiority of the FOC.

4 Conclusion

This article deals with prediction and avoidance of limit cycles generated by a dead zone in SISO servo systems. The prediction is committed to the describing function approach. The limit cycle avoidance is a remarkable achievement of a new, two-stages, FOC that provides nearly constant, high phase lead values within an interval around the frequency of the provided maximum lead. The controller shapes the Nyquist plot of the compensated system so as to respect robustness constraints based on a given distance from the describing function plot. Although the design approach is based on the classical theory of the describing function and Nyquist plots, it is remarked that classical techniques are still useful in the engineering practice [41]. The controller is implemented by approximating irrational transfer functions through a simple, efficient technique providing reduced order transfer functions. Such approximation is necessary for applying FOC to real systems but control performance and robustness is not weakened. The simplicity and efficiency make the controller acceptable to the engineering practice, for example, in many industrial applications where control loops are negatively affected by nonlinearities (dead zone, saturation, and backlash). Namely, in this article, the controller is designed for nonlinear systems including a dead zone element and a linear plant, which is a servo system for associated applications. However, the developed method can be extended to other systems including different nonlinear elements and/or different linear plants. This analysis will be the focus of future work.

Acknowledgments: The author would like to thank the Associate Editor and the anonymous Reviewers for their valuable comments that helped to improve the article.

Funding information: The author states no funding is involved.

Author contributions: The author has accepted responsibility for the entire content of this manuscript and approved its submission.

Conflict of interest: The author states that there is no conflict of interest.

Data availability statement: Data sharing is not applicable to this article as no datasets were generated or analyzed during the current study.

References

[1] Tao G, Lewis FL. Adaptive control of nonsmooth dynamic systems. New York (NY), USA: Springer-Verlag; 2001.
[2] Zuo Z, Ju X, Ding Z. Control of gear transmission servo systems with asymmetric deadzone nonlinearity. IEEE Trans Contr Syst Technol. 2016;24(4):1472–9.
[3] Tao G, Kokotovic PV. Adaptive control of plants with unknown dead-zones. IEEE Trans Automat Contr. 1994;39(1):59–68.
[4] Tao G, Kokotovic PV. Discrete-time adaptive control of systems with unknown deadzones. Int J Control. 1995;61(1):1–17.
[5] Hu C, Yao B, Wang Q. Adaptive robust precision motion control of systems with unknown input dead-zones: A case-study with comparative experiments. IEEE Trans Ind Electron. 2011;58(6):2454–64.
[6] Selmic RR, Lewis FL. Deadzone compensation in motion control systems using neural networks. IEEE Trans Automat Contr. 2000;45(4):602–13.
[7] Kim J-H, Park J-H, Lee S-W, Chong EKP. A two-layered fuzzy logic controller for systems with deadzones. IEEE Trans Ind Electron. 1994;41(2):155–62.
[8] Magesh N, Saravanan A. Generalized differential transform method for solving RLC electric circuit of non-integer order. Nonlinear Eng. 2018;7(2):127–35.
[9] Kapoor M, Khosla S. An iterative approach using Sawi transform for fractional telegraph equation in diversified dimensions. Nonlinear Eng. 2023;12:20220285.
[10] Oustaloup A, Mathieu B, Lanusse P. The CRONE control of resonant plants: Application to a flexible transmission. Eur J Control. 1995;1(2):113–21.

[11] Oustaloup A, Moreau X, Nouillant M. The CRONE suspension. Control Eng Pract. 1996;4(8):1101–8.
[12] Podlubny I. Fractional-order systems and $PI^{\lambda}D^{\mu}$-controllers. IEEE Trans Automat Contr. 1999;44(1):208–14.
[13] Lurie BJ. Three-parameter tunable tilt-integral-derivative (TID) controller. US patent US5371670, 1994.
[14] Raynaud H-F, Zergaínoh A. State space representation for fractional order controllers. Automatica. 2000;36(7):1017–21.
[15] Monje CA, Vinagre BM, Feliu V, Chen YQ. Tuning and auto-tuning of fractional order controllers for industry applications. Control Eng Pract. 2008;16(7):798–812.
[16] Caponetto R, Dongola G, Pappalardo F, Tomasello V. Auto-tuning and fractional order controller implementation on hardware in the loop system. J Optim Theory Appl. 2013;156(1):141–52.
[17] Abbisso S, Caponetto R, Diamante O, Fortuna L, Porto D. Non-integer order integration by using neural networks. ISCAS 2001 - The 2001 IEEE International Symposium on Circuits and Systems; 2001 May 6–9; Sydney, NSW, Australia. IEEE, 2001. p. 688–91.
[18] Calderon AJ, Vinagre BM, Felix V. On fractional sliding mode control. 7th Portuguese Conference on Automatic Control (CONTROLO 2006); 2006 Sep 11–13; Lisbon, Portugal.
[19] Efe MO. Fractional order sliding mode controller design for fractional order dynamic systems. Guvenc ZB, Baleanu D, Tenreiro Machado JA, editors. New trends in nanotechnology and fractional calculus applications. Dordrecht, Germany: Springer Verlag; 2010. p. 463–70.
[20] Jakovljević B, Pisano A, Rapaić MR, Usai E. On the sliding-mode control of fractional-order nonlinear uncertain dynamics. Int J Robust Nonlinear Control. 2015;26(4):782–98.
[21] Pisano A, Rapaić MR, Jeličić ZD, Usai E. Sliding mode control approaches to the robust regulation of linear multivariable fractional-order dynamics. Int J Robust Nonlinear Control. 2010;20(18):2045–56.
[22] Petráš I. Fractional-order nonlinear systems - modeling, analysis and simulation. Heidelberg Berlin, Germany: Springer-Verlag; 2011.
[23] Singh AK, Yadav VK, Das S. Comparative study of synchronization methods of fractional order chaotic systems. Nonlinear Eng. 2016;5(3):185–92.
[24] Rajagopal K, Karthikeyan A, Duraisamy P. Chaos suppression in fractional order permanent magnet synchronous generator in wind turbine systems. Nonlinear Eng. 2017;6(2):79–87.
[25] Caponetto R, Maione G, Sabatier J. Fractional-order control: a new approach for industrial applications (Editorial). Control Eng Pract. 2016;56:157–8.
[26] Boutayeb M, Darouach M. Recursive identifiation method for MIS0 Wiener-Hammerstein model. IEEE Trans Automat Contr. 1995;40:287–91.
[27] Dotoli M, Maione G, Naso D, Turchiano B. Genetic identification of dynamical systems with static nonlinearities. In: Embrechts MJ, VanLandingham HF, Ovaska SJ, editors. SMCia 2001 – Proceedings of the 2001 IEEE Mountain Workshop on Soft Computing in Industrial Applications; 2001 June 25–27; Blacksburg (VA), USA; IEEE, 2001. p. 65–70.
[28] Ogata K. Modern control engineering. Englewood Cliffs (NJ), USA: Prentice-Hall, Inc.; 1970.
[29] Nagrath IJ, Gopal M. Control systems engineering. New Delhi, India: Wiley Eastern Limited; 1975.
[30] Maione G. On a new class of multistage fractional-order phase-lead compensators. In: Babiarz A, Czornik A, Klamka J, Niezabitowski M, editors. Theory and Applications of Non-integer Order Systems - 8th Conference on Non-integer Order Calculus and Its Applications; 2016 Sep 20-21; Zakopane, Poland. Lecture Notes in Electrical Engineering. Vol. 407. Cham, Switzerland: Springer; 2017. p. 215–25.
[31] Lino P, Maione G. Realization of new robust digital fractional-order compensators. In: Dochain D, Henrion D, Peaucelle D, editors. Proceedings of the 20th IFAC World Congress; 2017 Jul 9-14; Toulouse, France. IFAC PapersOnLine, 2017;50–1:8580–5.
[32] Maione G. Multiple fractional networks for robust control design. Proceedings of the 2017 European Conference on Circuit Theory and Design (ECCTD); 2017 Sep. 4–6; Catania, Italy. IEEE, 2017. p. 1–4.
[33] Henrici P. Applied and computational complex analysis. Vol. 1: Power series, integration, conformal mapping, location of zeros. New York (NY), USA: John Wiley & Sons; 1974.
[34] Korn GA, Korn TM. Mathematical handbook for scientists and engineers: Definitions, theorems, and formulas for reference and review. New York (NY), USA: McGraw-Hill; 1961.
[35] Charef A, Sun HH, Tsao YY, Onaral B. Fractal system as represented by singularity functions. IEEE Trans Automat Contr. 1992;37(9):1465–70.
[36] Maione G. Continued fractions approximation of the impulse response of fractional order dynamic systems. IET Control Theory App. 2008;2(7):564–72.
[37] Maione G. Conditions for a class of rational approximants of fractional differentiators/integrators to enjoy the interlacing property. In: Bittanti S, Cenedese A, Zampieri S, editors. Proceedings of the 18th IFAC World Congress (IFAC 2011); 2011 Aug 28–Sep. 2; Milan, Italy. IFAC PapersOnLine: Vol. 18, Part 1, 2011. p. 13984–9.
[38] Adamy J. Nichtlineare systeme und regelungen. 2., bearbeitete und erweiterte auflage. Berlin, Germany: Springer Vieweg; 2009.
[39] Khalil HK. Nonlinear systems. 2nd ed., Upper Saddle River (NJ), USA: Prentice-Hall, Inc.; 1996. p. 454–60.
[40] Gelb A, Vander Velde WE. Multiple-input describing functions and nonlinear system design. New York (NY), USA: McGraw-Hill; 1968.
[41] Vukić Z, Kuljača L, Donlagić D, Tešnjak S. Nonlinear control systems. Control engineering series. New York (NY), USA: Marcel Dekker, Inc.; 2003.